

## Study on Manganese Dioxide/Loofah-Activated Carbon Supercapacitors

Lin Hu\*, Yating Pan, Shuai Liu, Lifang Jiang, Qujin Cui, Yijia Huang, Juan Tang, Jianping Liu<sup>1</sup>, Wenyuan Xu

School of Material Science and Engineering, East China JiaoTong University, Nanchang 330013, China;

\*E-mail: [Hulin21@hotmail.com](mailto:Hulin21@hotmail.com)

*Received: 25 March 2020 / Accepted: 8 June 2020 / Published: 10 July 2020*

---

The selection of appropriate carbon and loading materials and their corresponding preparation methods is necessary for obtaining high-quality supercapacitors. This paper used loofah as a raw material to prepare a kind of super activated carbon with a large specific surface area. Manganese dioxide was precipitated on the super activated carbon of the loofah using a solution precipitation method to prepare a manganese dioxide/super activated carbon composite electrode material. Scanning electron microscopy and X-ray diffraction were used to characterize the composite electrode materials. It was found that the loofah activated carbon had a porous composite structure, and manganese dioxide was loaded on the activated carbon as an amorphous structure. Cyclic voltammetry (CV), constant current charge and discharge (GCD), and AC impedance methods were used to study the electrochemical behaviour of the prepared composite electrode materials in KOH and Li<sub>2</sub>SO<sub>4</sub> electrolytes. The manganese dioxide/super activated carbon composite electrode material was used to assemble a supercapacitor, and its specific energy and specific power were measured by constant current charge and discharge. The electrochemical stability was tested by the application of multiple cycles of high current charge and discharge. When the electrolyte was a 6.0 mol/L potassium hydroxide solution, the current density was 1.25 A/g, and the measured specific capacitance was as high as 472.66 F/g.

---

**Keywords:** supercapacitors; activated carbon; manganese oxide; composite materials; electrochemical properties

### 1. INTRODUCTION

Supercapacitors are used as energy storage in many fields, such as cars, trains, tanks, ships, toys, satellites, and power storage, due to their high power density, fast charge and discharge, excellent working conditions at low temperatures, long cycle life, and environmental friendliness [1-3]. The main components of practical supercapacitors are the case, electrolyte, separator and electrode materials. The quality of the electrode material is directly related to the capacitance of the capacitor,

the charge and discharge characteristics, and the cycle life. The electrode materials that have been developed so far are mainly carbon materials [4-7] or the loading of metal oxides, hydroxides [8-10] or conductive polymers [11-13] on carbon materials. Pure carbon materials constitute supercapacitors, and activated carbon loaded with metal oxides, hydroxides or conductive polymers is used to form pseudocapacitors [14]. There are abundant sources of carbon materials for preparing supercapacitors. Coconut shells [15], durian shells [16], straw [17], corn cobs [18], and raw mineral materials such as coal tar and coal powder have been studied. There have also been reports on the use of graphene [19], carbon nanotubes [20], carbon nanofibres [21], and carbon nanoparticles [22] to prepare supercapacitors. Plant-derived carbon materials have the advantages of a large specific surface area and long cycle life, along with being easily available at a low price. They have been extensively studied and applied in the energy storage of supercapacitors [23-25]. Loofah has a unique structure and an abundance of pore channels. The use of loofah as a raw material for the preparation of loofah activated carbon takes advantage of its wide range of sources, low price, and convenient preparation, which can effectively reduce the cost of supercapacitor production. More importantly, activated carbon made from loofah has a large specific surface area. In the preparation of pseudocapacitors composed of rubidium oxide, ruthenium oxide and vanadium oxide, they have a high unit gravimetric capacity but are expensive. If manganese dioxide is supported on loofah activated carbon, because of the rich source of manganese dioxide, it becomes possible to obtain a cost-effective supercapacitor that still demonstrates a satisfactory specific capacitance [26, 27]. This article uses loofah as a raw material to prepare super activated carbon and then manganese dioxide is loaded on its surface. The hope is to provide a reference example for research of supercapacitors with high specific capacitance, low cost and high stability.

## 2. MATERIALS AND METHODS

### 2.1 Materials and Apparatus

A tablet machine, an electrochemical workstation, a battery tester, a muffle furnace, a vacuum drying oven, a magnetometer, and an electronic balance were used [28]. Ethanol (analysis), fine PTFE powder, potassium hydroxide (analysis), sodium hydroxide, potassium permanganate (analysis), manganese sulfate monohydrate (analysis) and homemade activated carbon powder were obtained and used.

### 2.2 Preparation of Activated Carbon Powder

Sheared biomaterials were cleaned, dried, and carbonized at 400°C. Solid hydroxide was then added to the carbonized biomaterial in a 1:3 ratio and placed in a muffle furnace (840°C, 10 minutes), where it was activated. The activated carbon powder was obtained by immersing the biochar into a solution of dilute hydrochloric acid, which was followed by pumping and washing until it was neutral; then, the sample was dried [28].

### 2.3 Preparation of the MnO<sub>2</sub>/Activated Carbon Composite Material

Briefly, 0.150 g of potassium permanganate and 0.240 g of manganese sulfate monohydrate were weighed to make solutions; additionally, 0.500 g of activated carbon powder was weighed. The activated carbon powder was added to the potassium permanganate solution and stirred to make the activated carbon powder uniformly dispersed. Then, the solution was added to the manganese sulfate solution with stirring. The addition of manganese sulfate solution was controlled to 5-8 minutes. After the addition, stirring was continued for 30 minutes to obtain a manganese oxide/activated carbon composite material, which was suction filtered and washed to neutrality. The MnO<sub>2</sub>/activated carbon composite material was obtained through negative pressure filtration, water washing to neutrality, and drying [28].

### 2.4 Preparation of the Electrode

A round nickel foam was weighed. Then, a mixture of the composite material, acetylene black and fine PTFE powder at a ratio of 8:1:1 was prepared and applied to the round nickel foam nickel. The material was air dried. This was the prepared electrode plate [28].

## 3. RESULTS AND DISCUSSION

### 3.1. SEM Analysis Test

#### (1) SEM Analysis Test of the Activated Carbon Material

Scanning electron microscopy is an intuitive method to observe the surface characteristics of objects. In this experiment, an s-3400 high-resolution scanning electron microscope was used to scan the appearance of the activated carbon material, and the experimental voltage was 15 kV. Figs. 1A and 1B are shown below [28]:

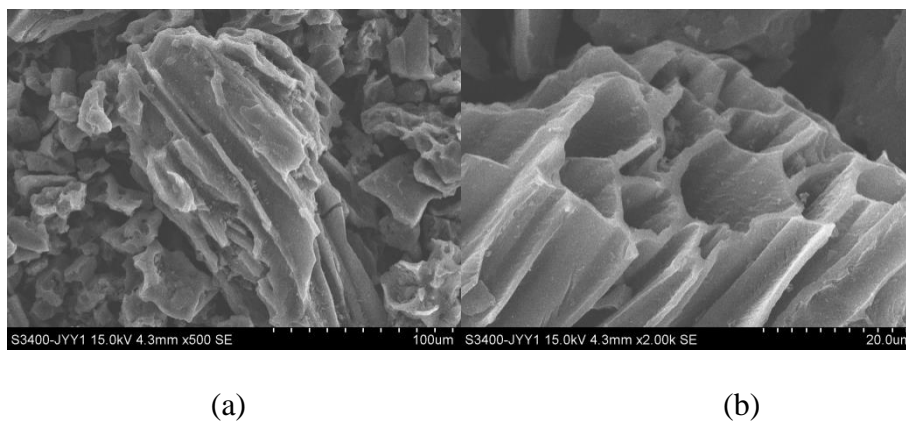


**Figure 1.** SEM characterization of the loofah activated carbon.

It can be clearly seen that the activated carbon has many microporous structures.

(2) SEM Analysis Test of the Manganese Dioxide/Activated Carbon Composites

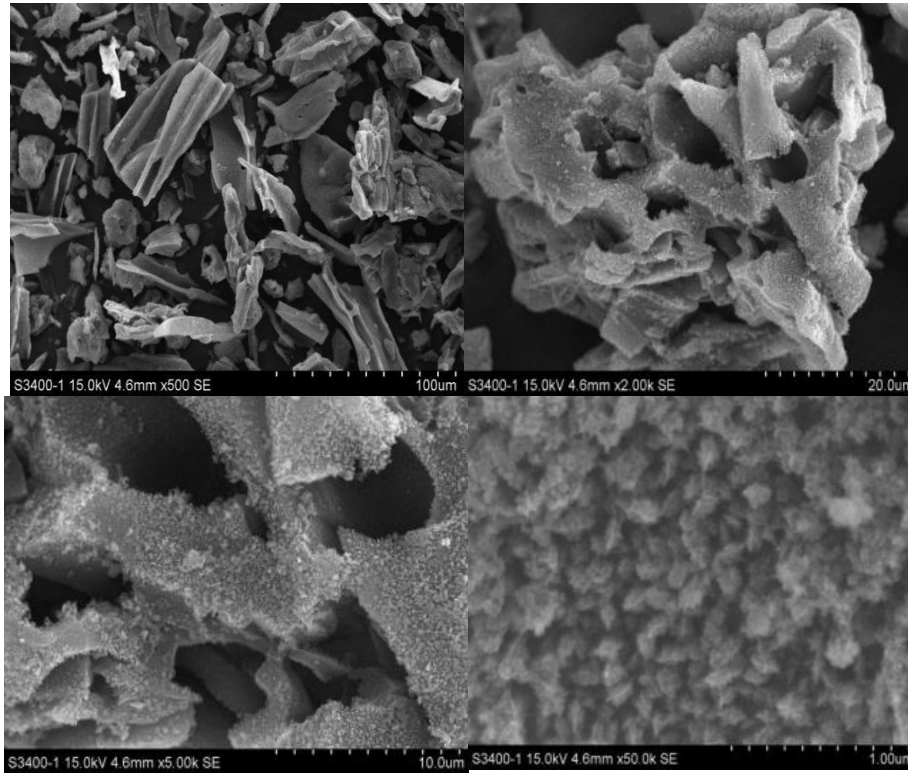


Figure 2. SEM characterization of the manganese dioxide/activated carbon composites.

From Fig. 2, manganese oxide particles adhered to the surface of the activated carbon and around the pores. Thus,  $MnO_2$  was successfully supported on the activated carbon.

3.2 X-ray Diffraction Analysis

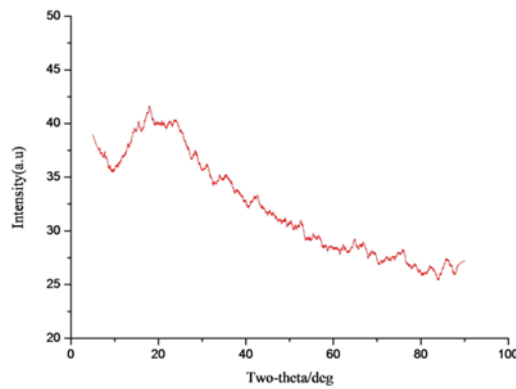


Figure 3. XRD curve of the  $MnO_2$ /activated carbon composite material.

The diffraction pattern of the MnO<sub>2</sub>/activated carbon composite material is shown below in Fig. 3. It can be seen that the peak corresponding to manganese oxide is not very sharp, and there are a few scattered peaks. The generated manganese oxide should have an amorphous structure, but the amorphous structure is conducive to the entry and exit of ions and energy storage. The capacitance is relatively large [28].

### 3.3 Two-Electrode System Test

The charge value is expressed as  $I \cdot \Delta t$ ,  $\Delta t$  is the selected time period,  $m$  is the mass of the composite material, and  $\Delta V$  is the voltage difference between the start time and the end time [24]. The formula for the electrode material is shown as (1):

$$C = \frac{I \cdot \Delta t}{m \cdot \Delta V} \quad (1)$$

By changing the current value, we determined the difference in electrochemical performance between different currents. Then, the constant current charging and discharging charts at currents of 2 mA and 9 mA are listed. From Fig. 4 and Fig. 5, the specific capacitance was 171.03 F/g, 103.56 F/g, 328.26 F/g, 268.18 F/g. Compared with Fig. 4(a) and Fig. 4(b), we can see that the larger the current, the smaller the specific capacitance. As the current increases, the charge transfer speed will increase, but the charge on the surface and the channel of the activated carbon will decrease; additionally, the specific capacitance will decrease. We observed that the charge-discharge curve is not very smooth. This is due to the increase in the specific capacitance due to the occurrence of a redox reaction and the generation of false capacitance. After comparing the figures and values of 1.0 mol/L lithium sulfate and 6.0 mol/L potassium hydroxide, the latter has greater specific capacitance when used as an electrolyte [28].

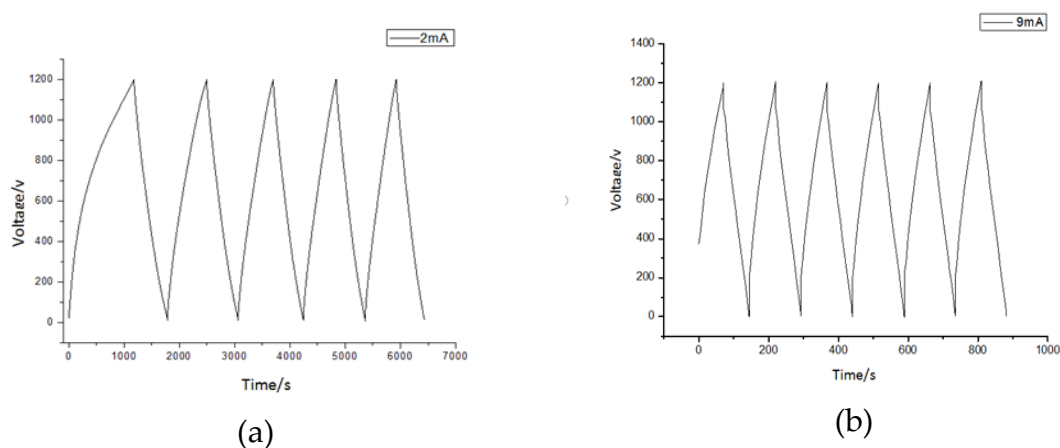


**Figure 4.** Constant current charge and discharge diagram of the supercapacitors made of manganese dioxide/activated carbon composite materials in a 1.0 mol/L lithium sulfate electrolyte: (a) charge and discharge curve at a current of 2 mA and (b) charge and discharge curve at a current of 9 mA.

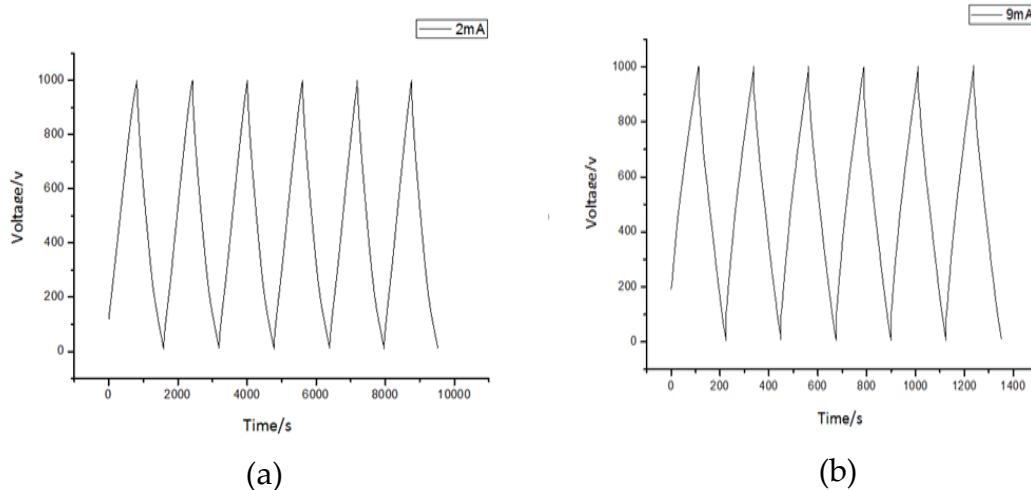


**Figure 5.** Constant current charge and discharge diagram of the supercapacitors made of manganese dioxide/activated carbon composite materials in a 6.0 mol/L potassium hydroxide electrolyte: (a) charge and discharge curve at a current of 2 mA and (b) charge and discharge curve at a current of 9 mA.

### 3.4 Three-Electrode System Test

When performing a three-electrode constant current charge and discharge test, the measurement is from a small current of 3 mA to a large current of 10 mA, and the graphs of the small current of 3 mA and the large current of 10 mA are shown in the following figures:

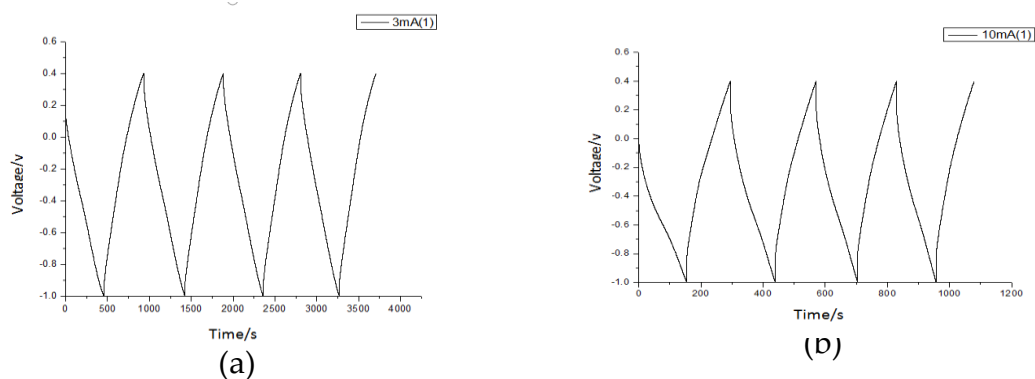


**Figure 6.** Constant current charge and discharge diagram of the supercapacitors made of manganese dioxide/activated carbon composite materials in a 1.0 mol/L lithium sulfate electrolyte: (a) charge and discharge curve at a current of 3 mA and (b) charge and discharge curve at a current of 10 mA.

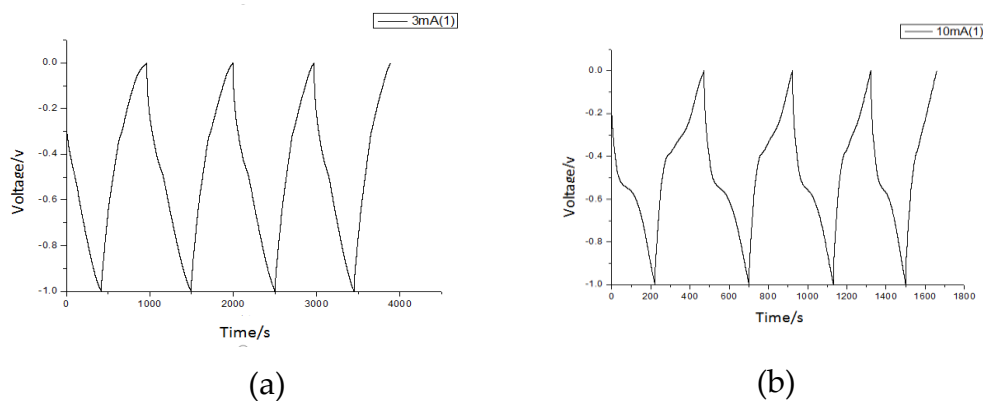
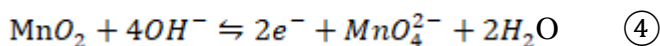
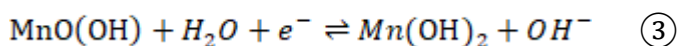
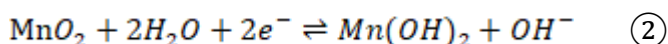
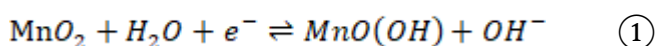


**Figure 7.** Constant current charge and discharge diagram of the supercapacitors made of manganese dioxide/activated carbon composite materials in a 6.0 mol/L potassium hydroxide electrolyte: (a) charge and discharge curve at a current of 3 mA and (b) charge and discharge curve at a current of 10 mA.

Fig. 7(b) shows that there is an approximate plateau. This is because a redox reaction has occurred, and charge transfer and storage results in a pseudocapacitance, which improves the specific capacitance. After processing the data, the maximum specific capacitance measured when the electrolyte is 6.0 mol/L potassium hydroxide and the current density is 1.25 A/g is 472.66 F/g; when the electrolyte is 1.0 mol/L lithium sulfate, the current density is 1.14 A/g. The maximum specific capacitance measured is 172.19 F/g. The reason is because the lithium sulfate solution is a neutral solution, which is not conducive to the reversibility of the redox reaction, so the specific capacitance is not high; the potassium hydroxide solution is an alkaline solution, which is conducive to the reversibility of the redox reaction, so the process occurs. The degree of redox reaction is stronger in the latter than the former, and the specific capacitance is also higher. The equations of the reaction mechanism in an alkaline solution may appear as the following (①, ②, ③, ④)[29-31]:



### 3.5 Cyclic Voltammetry Test

Different curves were obtained by changing the scan rate. The integrated area is  $S$ ,  $m$  is the mass of the electrode material,  $\Delta E$  is the voltage difference, and  $V$  is the scan rate [32]. The formula for the specific capacitance through the use of an integral method can be expressed as (2):

$$C = \frac{S}{2 \cdot m \cdot V \cdot \Delta E} \quad (2)$$

$\text{Li}_2\text{SO}_4$  solution (1 mol/L) and  $\text{KOH}$  solution (6.0 mol/L) are used as the electrolytes, and the scanning rate is gradually increased from 5 mV/s to 10 mV/s. Fig. 8(a) and Fig. 8(b) show that as the scan rate increases, the capacitance of the supercapacitor decreases. The reason is because when the current increases, the charge transfer speed also increases. Thus, the charge storage on the surface of

the activated carbon and in the pores decreases, and the specific capacitance also decreases. Moreover, it can be observed that the charge-discharge curve is no longer a straight line, especially the discharge curve. The obvious curve becomes flattened, indicating that a redox reaction has occurred, so pseudocapacitance behaviour has been generated, and thus, the specific capacitance has also increased [28].

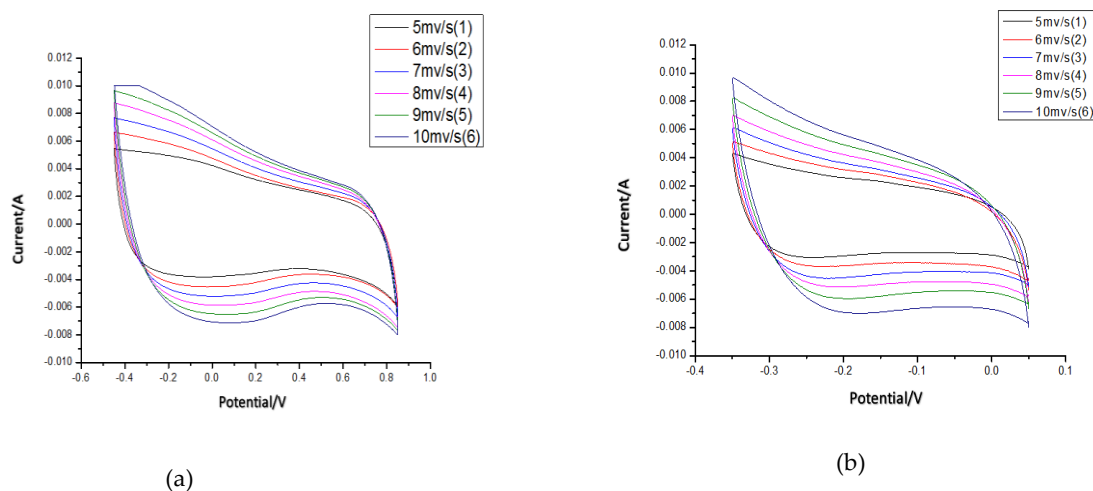


**Figure 8.** Frequency distribution of the cyclic voltammetry curves with various scanning rates: (a) 1 mol/L  $\text{Li}_2\text{SO}_4$  electrolyte and (b) 6.0 mol/L KOH electrolyte.

### 3.6. Impedance Test

An increase in impedance directly leads to the failure of the capacitor [33]. The following is the impedance diagram tested by the three-electrode system, which is composed of nickel foam as the working electrode, a calomel electrode as the reference electrode and a platinum electrode as the auxiliary electrode.

The equivalent resistance can be obtained by intersecting the line with the axis. Fig. 9 (a) is the impedance measured when the electrolyte is 1.0 mol/L lithium sulfate, and Fig. 9 (b) is the impedance measured when the electrolyte is 6.0 mol/L potassium hydroxide. It can be seen from the figure that the equivalent internal resistance of Fig. 9(a) is approximately  $11.80 \Omega$ , and the equivalent internal resistance of Fig. 9(b) is approximately  $12.13 \Omega$ . The main reason is that the electrode materials and electrolytes have intrinsic internal resistance and contact resistance, that can be affected by temperature and storage time. To reduce the internal resistance, the electrode material must be optimized, and a suitable electrolyte should be selected.

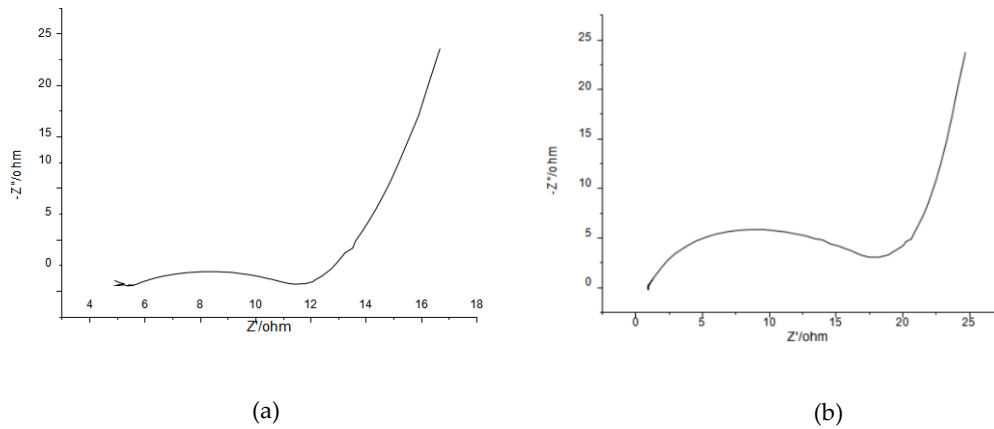


**Figure 9.** Impedance test: (a) 1 mol/L Li<sub>2</sub>SO<sub>4</sub> electrolyte and (b) 6.0 mol/L KOH electrolyte.

### 3.7. Cycle Life Test

#### 3.7.1 Assembly of the Supercapacitors

An appropriate amount of electrolyte is added to the electrode plate. The electrolyte prepared in this experiment is a 6.0 mol/L potassium hydroxide solution. The membrane is immersed in the electrolyte for several minutes, and the excess electrolyte is dried [8]. A plate-film-plate structure is then pressed into a battery housing with the use of a tablet machine at a pressure of 10 KPa [28].

To test the stability of the button cell, a charge-discharge experiment of 1,000 cycles was performed. As shown in Fig. 10, the supercapacitor has stable performance and a long cycle life. The specific capacitance of 100, 300, 600, 800, and 1000 cycles was 114.6 F/g, 111.3 F/g, 111.5 F/g, 110.2 F/g, and 111.1 F/g, respectively; furthermore, the 96.95% of the initial capacitance is retained.

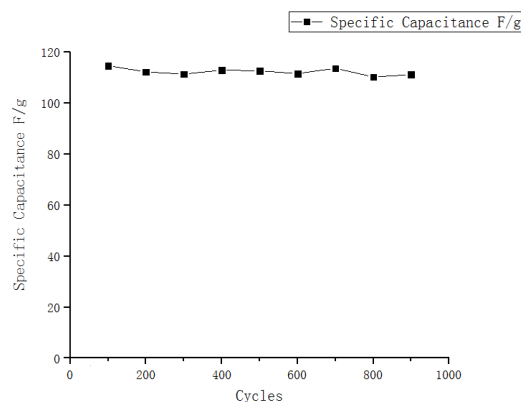


**Figure 10.** Frequency distribution of the specific capacitance over an increasing number of cycles.

### 3.8. Comparison with other similar supercapacitors

Manganese has several stable oxides, such as  $\text{MnO}_2$ ,  $\text{Mn}_3\text{O}_4$ , which has diverse crystal structures, defect chemistry, morphology, porosity and textures. They possess rich electrochemical properties, and are highly recommended to use for supercapacitor electrodes [34]. To visualize the electrochemical properties of manganese oxides fabricated materials, the comparison of specific capacitance and cycle life of supercapacitors using  $\text{MnO}_2/\text{Mn}_3\text{O}_4$ -based electrodes is shown. Impressively,  $\text{MnO}_2/\text{Loofah-Activated Carbon}$  in this work outperforms many  $\text{MnO}_2/\text{Mn}_3\text{O}_4$ -based electrode materials in recently reports, such as the ones listed in Table 1.

**Table 1.** Comparison of the properties of our sample with other similar supercapacitors

Samples	Electrolyte	Specific capacitance	Number of cycles	Capacity retention (%)	References
L-AC@ $\text{MnO}_2$	6 M KOH	$248 \text{ F} \cdot \text{g}^{-1}$ ( $1 \text{ A} \cdot \text{g}^{-1}$ )	3000	79.3	[35]
a- $\text{MnO}_2$ NWs@d- $\text{MnO}_2$ NSs	6 M KOH	$276.9 \text{ F} \cdot \text{g}^{-1}$ ( $1 \text{ A} \cdot \text{g}^{-1}$ )	10000	98.1	[36]
Graphene/ $\text{MnO}_2$	1 M $\text{Na}_2\text{SO}_4$	$320 \text{ F} \cdot \text{g}^{-1}$ ( $0.5 \text{ A} \cdot \text{g}^{-1}$ )	2000	84	[37]
Rice husks/Hierarchically porous $\text{MnO}_2$	0.5M $\text{Na}_2\text{SO}_4$	$210.3 \text{ F} \cdot \text{g}^{-1}$ ( $0.5 \text{ A} \cdot \text{g}^{-1}$ )	5000	80.2	[38]
$\text{Mn}_3\text{O}_4$ nanoflakes/rGO	1M $\text{Na}_2\text{SO}_4$	$351 \text{ F} \cdot \text{g}^{-1}$ ( $0.5 \text{ A} \cdot \text{g}^{-1}$ )	10000	80.1	[39]
cobalt-doped $\text{MnO}_2/\text{GO}$	1 M $\text{Na}_2\text{SO}_4$	$397 \text{ F} \cdot \text{g}^{-1}$ ( $0.5 \text{ A} \cdot \text{g}^{-1}$ )	4000	97.5	[40]
$\text{MnO}_2/\text{Loofah-Activated Carbon}$	6M KOH	472.66 $\text{F} \cdot \text{g}^{-1}$ ( $1.25 \text{ A} \cdot \text{g}^{-1}$ )	1000	96.95	This work

#### 4. CONCLUSIONS

Activated carbon is obtained from loofah, which is a biological material, and a MnO<sub>2</sub>/activated carbon composite is produced by direct precipitation. Compared with 1.0 mol/L lithium sulfate, the 6.0 mol/L potassium hydroxide has a higher specific capacitance when used as an electrolyte at a current density of 1.25 A/g; specifically, the capacitance is as high as 472.66 F/g, and 96.95% of the initial specific capacitance is retained after 1000 cycles. The prepared supercapacitors have the characteristics of environmental friendliness, high charge and discharge efficiency, and long cycle life; thus, they have broad application prospects.

#### ACKNOWLEDGMENTS

The authors gratefully acknowledge the funding of the National Natural Science Foundation of China (nos. 21871049) and the Natural Science Foundation of Jiang Xi Province of China (20181BAB204012).

#### References

1. Q.Z. Zhang, D. Zhang, Z. C. Miao, X. Li. Zhang, and S. L. Chou, *Small*, 14(2018)1702883. doi.org/10.1002/sml.201702883
2. H.C. Yang, R.Y. Cao, P.X. Sun, X.L. Deng, S.W. Zhang, and X.J. Xu, *Appl. Surf. Sci.*, 458 (2018) 893. doi.org/10.1016/j.apsusc.2018.07.149
3. M. Sellali, S. Abdeddaim, A. Betka, A. Djerdir, S. Drid, and M. Tiar, *ISA Trans.*, 95(2019)243. doi.org/10.1016/j.isatra.2019.04.029
4. J. Hou, C. Cao, F. Idrees, and X. Ma, *ACS Nano*, 9(2015)2556. DOI:10.1021/nn506394r
5. T.Y. Kim, G.J. Jung, S.Yoo, K.S. Suh and R.S. Ruoff, *ACS Nano*, 7(2013)6899. DOI:10.1021/nn402077v
6. T. Lin, I.W. Chen, F.X. Liu, C.Y. Yang, H.Bi, F.F. Xu and F. Q. Huang, *Science*, 350(2015)1508. DOI:10.1126/science.aab3798
7. J.H. Hou, K. Jiang, R. Wei, M. Tahir, X.G. Wu, M. Shen, X.Z. Wang and C.B. Cao, *ACS Appl. Mater. Interfaces*, 9(2017)30626. DOI: 10.1021/acsami.7b07746
8. W.T. Sun, L. Xiao, and X. Wu, and *J. Alloy. Comp.*, 772(2019)465. doi.org/10.1016/j.jallcom.2018.09.185
9. L. Wang, H.M. Ji, S.S. Wang, L.J. Kong, X.F. Jiang, and G. Yang, *Nanoscale*, 5(2013)3793. DOI:10.1039/C3NR00256J
10. H. Jiang, T. Zhao, C.Z. Li, and J. Ma, *J. Mater. Chem.*, 21(2011,)3818. DOI:10.1039/c0jm03830j
11. G.A. Snook, P. Kao and A.S. Best, *J. Power Sources*, 196(2011) 1. DOI:10.1016/j.jpowsour.2010.06.084
12. D.P. Dubal, S.H. Lee, J.G. Kim, W.B. Kim and C.D. Lokhande, *J. Mater. Chem.*, 12(2012)3044. DOI: 10.1039/c2jm14470k
13. D.P. Zhao, H.Q. Liu and X. Wu, *Nano Energy*, 57(2019)363. DOI:10.1016/j.nanoen.2018.12.066
14. A. Borenstein, O. Hanna , R. Attias, S. Luski, T. Brousseb and D. Aurbach, *J. Mater. Chem. A*, 5 (2017)12653. DOI:10.1039/C7TA00863E
15. M. Galinski, K. Babel and K. Jurewicza, *J. Power Sources*, 228(2013)83. DOI: 10.1016/j.jpowsour.2012.11.048
16. J.P. Tey, M. A. Careem, M. A. Yarmo and A. K. Arof, *Ionics*, 22(2016)1209. DOI: 10.1007/s11581-016-1640-2

17. W. Du, Z. Zhang, L. Du, X.Y. Fan, Z.W. Shen, X.R. Ren, Y.P. Zhao, C.Z. Wei and S.H. Wei, *J. Alloys Compd.*, 707(2019)1031. doi.org/10.1016/j.jallcom.2019.05.207
18. M. Gopiramanb, D. Denga, B.S. Kim, I.M. Chung and I.S. Kim, *Appl. Surf. Sci.*, 409(2017)52 . doi.org/10.1016/j.apsusc.2017.02.209
19. V. Sridhar, H. Park, *J. Alloys Compd.*, 808(2019)151748. doi.org/10.1016/j.jallcom.2019.151748
20. J. Miao, X. Dong, Y.L. Xu, Z.Z. Zhai, L.H. Zhang, B. Ren and Z.F. Liu, *Org. Electron.*, 73(2019)304. doi.org/10.1016/j.orgel.2019.06.025
21. E. Stojanovska, A. Kilic, *Journal of Energy Storage*, 26(2019)100981. doi.org/10.1016/j.est.2019.100981
22. K. Mohanapriya, N. Jha, *Electrochim. Acta*, 324(2019)134870. doi.org/10.1016/j.electacta.2019.134870
23. P. Simon, Y. Gogotsi, *Acc. Chem. Res.*, 46(2013)1094. DOI:10.1021/ar200306b
24. X.Q. Li, L. Chang, S.L. Zhao, C.L. Hao, C.G. Lu, Y.H. Zhu and Z.Y. Tang, *Acta Phys. Chim. Sin.*, 33(2017)130. DOI:info:doi/10.3866/PKU.WHXB201609012
25. T. Qi, S.F. Huang, *Journal of Yanshan University*, 5(2015)377. TQ127.11;TM53
26. P. Thomas, C. Wei , M. Rafie, B. Johan, *Journal of Analytical and Applied Pyrolysis*, 140(2019)54. doi.org/10.1016/j.jaap.2019.03.021
27. S. Song, Y. He, Y. Ruan, N. Jiang and B. Cheng, *Mater. Lett.*, 247(2019)82. doi.org/10.1016/j.matlet.2019.03.100
28. J. Wang, J.Q. Li, Q.J. Cui, G.X. Xu and L. Hu, *2018 2nd International Conference On Green Energy And Application*, 978-1-5386-5236-7/18/\$31.00 ©2018 IEEE.
29. Y. Ping, Z. Liu, J. Li, J. Han, Y. Yang, B. Xiong, P. Fang and C. He, *J. Alloys Compd.* 805 (2019) 822. doi.org/10.1016/j.jallcom.2019.07.125
30. S. Mothkuri, S. Chakrabarti, H. Gupta, B. Padya, T.N. Rao and P.K. Jain, *Mater. Today: Proc.* 26 (2020) 142. doi.org/10.1016/j.matpr.2019.03.236
31. H. Wang, Q. Fu and C. Pan, *Electrochim. Acta*, 312 (2019) 11. doi.org/10.1016/j.electacta.2019.04.178
32. X.Z. Sun, X. Zhang, D.C. Zhang, Y.W. Ma, *Acta Phys. Chim. Sin.*, 28(2012)367. doi:10.3866/PKU.WHXB201112131.
33. X.J. Lv, P. Zhu, *Micronanoelectronic Technology*, 33(2017)31. doi:10.13250/j.cnki.wndz.2017.01.006.
34. M. Toupin, T. Brousse and D. Be, *Chem. Mater.*, 14 (2002) 3946. DOI: 10.1021/cm020408q
35. H.L. Wei, X.N. Wang, D.M. Zhang, W. Du, X.Q. Sun, F.Y. Jiang and T.S. Shi, *J. Electroanal. Chem.*, 853(2019) 113561. doi.org/10.1016/j.jelechem.2019.113561
36. Z. Ma, G. Shao, Y. Fan, G. Wang, J. Song and D. Shen, *ACS Appl. Mater. Interf.*, 8(2016) 9050. DOI:10.1021/acsami.5b11300
37. A. Kumar, B. Wang, D. Su, Y. Wang, S. Chen, X. Zhang and G. Wang, *Mater. Chem. Phys.*, 143 (2014) 740 . DOI:10.1016/j.matchemphys.2013.10.008
38. C.J. Yuan, H.B. Lin, H.Y. Lu, E.D. Xing, Y.S. Zhang and B.Y. Xie, *Appl. Energy*, 178 (2016) 260. doi.org/10.1016/j.apenergy.2016.06.057
39. Z. Huang, S. Li, Z. Li, J. Li, G. Zhang, L. Cao and H. Liu, *J. Alloys Compd.*, 830(2020) 154637. doi.org/10.1016/j.jallcom.2020.154637
40. R. Nasser, G.F. Zhang, and J.M. Song, *Electrochim. Acta*, 345(2020) 136198. doi.org/10.1016/j.electacta.2020.136198